ORIGINAL PAPERS

Relationship between ozone and biologically relevant UV at 4 NDACC sites

Richard McKenzie[1] · Ben Liley[1] · Michael Kotkamp[1] · Alexander Geddes[1] · Richard Querel[1] ·
Scott Stierle[2] · Kathleen Lantz[2] · Steve Rhodes[3] · Sasha Madronich[4]

Abstract

Clouds and aerosols, as well as overhead ozone, can have large effects on ultraviolet (UV) irradiances. We use statistical methods to remove cloud effects and mean aerosol effects from spectral UV irradiance measurements to investigate the relationship between UV and total column ozone. We show that for fixed solar zenith angles (SZA), seasonal changes in ozone lead to marked changes in clear-sky UV irradiances. Such effects are larger at mid-latitudes than in the tropics. At mid-latitudes, the minimum ozone amount over the course of a year can be about 50 percent of its maximum, with the lowest values in autumn and the highest values in spring. These seasonal ozone changes lead to UV Index (UVI) values in autumn that can exceed those in spring at the same SZA by nearly a factor of two. Differences are even larger for UV spectra weighted by the action spectra for DNA-damaging UV, and for cutaneous previtamin D production. In some cases, the seasonal increase exceeds a factor of 4. The analysis experimentally demonstrates the limits of applicability of the concept of constant Radiative Amplification Factors (RAFs) for estimating effects of changes in ozone for some weighting functions. Changes in DNA-weighted UV and erythemally weighted UV are well represented by the published RAFs. However, there are large SZA dependencies in the case of UVB and vitamin D-weighted UV. For all weightings considered, RAFs calculated from the observations as a function of SZA show similar dependencies between sites, in good agreement with published values, independently of the ozone data source.

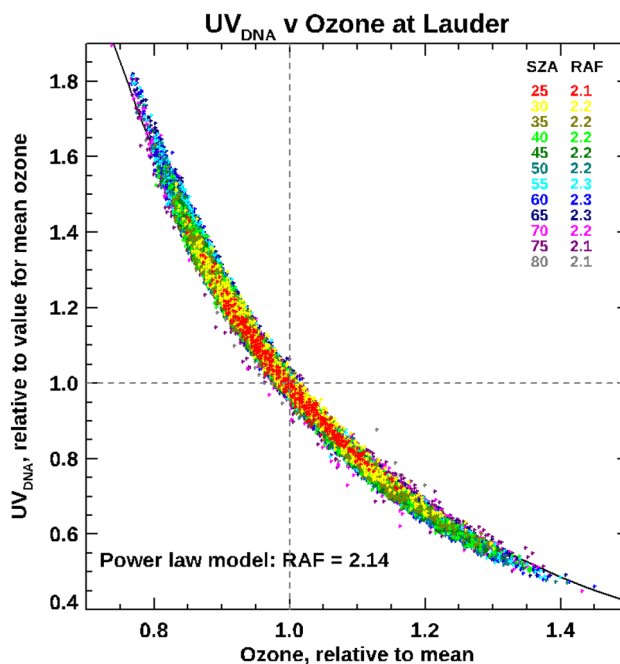✉ Richard McKenzie
  richard.mckenzie@niwa.co.nz

1 National Institute of Water & Atmospheric Research (NIWA), Lauder, New Zealand

2 NOAA, Boulder, CO, USA

3 Bureau of Meteorology, Melbourne, Australia

4 NCAR, Boulder, CO, USA

Graphical abstract

High quality measurements show that natural variations in ozone are responsible for huge variations in biologically damaging UV, with seasonal changes at fixed solar zenith angles sometimes exceeding a factor of four. The measured changes from thousands of spectra agree well with calculations over a wide range of solar zenith angles.

Keywords Ozone · UV · UV index · NDACC · Atmosphere · Health

1 Introduction

The dramatic effect of ozone changes on measured UV irradiance (hereafter referred to as 'UV') is very well demonstrated by a plot [1] that first appeared in the 1998 UNEP Assessment of the Environmental Impact of Ozone Depletion [2]. The now widely reproduced plot used UV measured under clear skies at fixed solar zenith angles (SZA) from several sites to highlight its dependence on total column ozone (hereafter referred to as 'ozone'), and showed that the observed change is well represented by model calculations. Strikingly, it showed that UV spectra weighted with the action spectra for erythema (i.e. erythemally weighted UV, or UV_{Ery} hereafter) can be more than doubled when the ozone amount is halved.

Since then there has been a huge increase in the availability of high-quality spectral UV data for such assessments. UV measurements undertaken and archived within the international Network for the Detection of Atmospheric Composition Change (NDACC) [3] provide one source of such data.

Here we extend the 1998 work [1], using long-term data from four NDACC sites, to investigate the geographical variability and the SZA dependence of the relationship between ozone and UV_{Ery}, using a much larger number

of measurements spanning a wide range of altitudes and latitudes and reporting them in terms of the more widely used UV Index (UVI), defined as $UV_{Ery}/(0.025\ \mathrm{Wm^{-2}})$ [4]. We show that, with care, these dependencies can be determined using the spectral irradiance data alone without recourse to supplementary sources, such as ozone data or other means to establish clear-sky conditions.

We also investigate the applicability and limitations of using calculated "Radiation amplification factors" (RAFs, defined below) to describe these changes in UV as a function of ozone. Further, we investigate the relationships for other weightings, including UVA (315–400 nm), UVB (280–315 nm), UV weighted by the action spectrum for DNA damage (UV_{DNA}) and UV weighted by the action spectrum for initiating the production of previtamin D (UV_{VitD}), a precursor to the production of blood serum 25(OH)D.

2 Radiation amplification factors

Biologically weighted UV irradiances (UV_{bio}) are usually defined by integration over wavelength λ,

$$UV_{bio}(O_3, \dots) = \int I(\lambda, O_3, \dots) A_{bio}(\lambda) \mathrm{d}\lambda, \qquad (1)$$

of the spectral irradiance $I(\lambda, O_3, \dots)$ multiplied (weighted) by a spectral sensitivity function or action spectrum $A_{bio}(\lambda)$ for the biological endpoint of interest, e.g. the induction of sunburn (erythema) in skin or cataract in eyes. The solar UV spectral irradiance that reaches Earth's surface—and hence UV_{bio}—depends on ozone (O_3), as well as on a host of other factors, including SZA, clouds, aerosols and local reflections. The dependence of UV_{bio} on ozone has been recognised at least since the pioneering work in the 1930s of Latarjet [5] who evaluated Eq. 1 with the action spectrum for erythema that had been measured earlier that decade by Coblentz et al. [6]. In the 1970s, increasing concerns about ozone depletion, in relation to both the proposed supersonic transport (SST) fleet [7] and CFC emissions [8], led to renewed interest in calculating how UV_{bio} would respond to reductions in stratospheric ozone. To facilitate such estimations, a sensitivity parameter dubbed the Radiation Amplification Factor (*RAF)* was defined [9–12] for small changes in O_3 (<10%), as the fractional (or %) change in UV relative to that of the O_3,

$$\frac{\Delta UV}{UV} = -RAF \frac{\Delta O_3}{O_3}. \qquad (2)$$

Since the dependence of UV on O_3 is expected to be monotonic and smooth on physical grounds, such a definition can always be made, but the *RAF* may or may not be constant over any practical variation of O_3 or other environmental factors. With the advent of the Antarctic ozone hole [13], the issue also arose whether RAFs could be used for much larger $\Delta O_3/O_3$. Direct integration of Eq. 1 was proposed after noticing, from numerical simulations, that RAFs for many action spectra remain near constant over relevant changes in O_3 or *SZA* [14–16], resulting in the power rule:

$$\frac{UV + \Delta UV}{UV} = \left(\frac{O_3 + \Delta O_3}{O_3} \right)^{-RAF}. \qquad (3)$$

Direct measurements of O_3 and DNA-damaging UV in Antarctica confirmed this relation, while use of Eq. 2 led to serious underestimation of the large UV enhancements [17]. Since then, extensive tabulations of RAFs have been calculated for various action spectra, including DNA damage, erythema induction, plant damage, and many other photobiological and photochemical processes [18, 19], and these continue to be used for rapid estimation of the effects of ozone changes on various processes. RAF-based estimations are obviously much faster than those utilising a full action spectrum, but are only useful if the RAF is approximately constant over the relevant conditions.

It was shown in 2003 [20] that the RAF is indeed nearly constant, over a wide range of ozone and SZA, if the action spectrum can be approximated by a simple exponential decay over the wavelengths of interest (ca. 300–330 nm). With this and a few other approximations, the integrand of Eq. 1 can be expressed as a Gaussian function whose analytical integration yields the power rule (Eq. 3) and the RAF is directly proportional to the decay rate (semilogarithmic slope) of the action spectrum. Micheletti et al. [20] also noted that constancy of the RAFs should not be expected when action spectra deviate from simple exponential decay. An extreme case is that of action spectra that are truncated, i.e., set to zero at wavelengths beyond which the signal becomes too small to measure; this can lead to overestimation of the RAF, particularly at low sun and high ozone, where longer wavelengths have larger relative contributions. Conversely, the erythema action spectrum becomes less steep at longer wavelengths, leading to smaller RAFs at low sun/high ozone.

Although the dependency of RAFs on ozone and SZA can be readily displayed in contour plots [20], it is difficult to extract quantitative estimates from these. More recently, a graphical method was developed to quantitatively show these dependencies (e.g. ref [21] see Fig. 6 on page 24 therein).

Experimental determinations of RAFs are relatively few, but already in 1991 it was shown that measured changes in UV_{Ery} as a function of ozone at Lauder agree well with those calculated from published RAFs [22]. In a follow-up study, using one year of spectral irradiance data from the high altitude Mauna Loa Observatory, it was shown that the RAF for erythema is slightly larger than predicted by the model (though just within experimental uncertainty limits) for small SZAs, but reduces below unity at larger SZAs [23]. As noted above that drop-off in RAF at large SZA (and in fact for large slant ozone column amounts) occurs because then relatively more of the UVA tail of the CIE spectrum contributes [20].

A few other studies have been carried out around the world to determine RAFs. For example, measurements at a high altitude observatory in Austria determined RAFs specific to RB meters and other narrowband filter instruments that were in use at the time [24]. The effect of clouds on the RAF for erythema was first determined from measurements in Spain [25], and in a follow-up study, data from the EPA network of Brewer radiometers were used to measure the effect of clouds on RAFs at several North American sites [26]. The first of these studies [25] showed that, while clouds tend to decrease absolute UV, they tend to increase its dependence on ozone, leading up to RAFs 20% larger, with largest increases for largest cloud optical depths. The second study [26] showed an RAF dependence on the 'clearness index', defined as the percent of clear-sky radiation

transmitted. The RAF was found to decrease for the lowest transmissions, but to increase by up to 20% for intermediate transmissions. Here we focus on the SZA dependence for clear skies.

3 Procedure

Typical spectral irradiances for clear skies at noon for Lauder are shown in the upper panel of Fig. 1. The steep drop in irradiance at shorter UVB wavelengths is due mainly to absorption by ozone. The absorption cross section of ozone is also shown [27]. Losses by Rayleigh scattering (not shown) become increasingly important at shorter wavelengths. Note that although there is considerable structure in ozone's absorption cross section in the UVA region, the spectral irradiance features there are due rather to Fraunhofer absorptions in the Sun's atmosphere. The UVI values for these summer and winter spectra are approximately 11 and 1, respectively.

In the middle panel of Fig. 1, the weighting function for erythema [28] is compared with those for damage to DNA [29], the production of previtamin D [30] and the boundary at 315 nm between the UVB and UVA regions.

Note that of these biological weightings, erythema is the only for which the contribution from wavelengths longer than 330 nm is significant. The biologically weighted irradiance, shown for several examples in the bottom panel of Fig. 1, is the integral over wavelength of the spectral irradiance multiplied by the weighting function. The former increases steeply with wavelength, while the latter decreases steeply. As has been shown elsewhere [31], the weighted irradiances are typically dominated by the contribution between 300 and 310 nm (with a displacement to slightly longer wavelengths in winter). At shorter wavelengths, irradiances are too small to contribute, while at longer wavelengths, the weighting functions become too small (noting that the upper two panels of Fig. 1 are plotted on logarithmic y-axes). Clearly, for weighting functions, like that for DNA damage, that increase more steeply with decreasing wavelength through the UVB region, the peak wavelength is shorter, and there will be a stronger dependence on the amount of ozone in the radiation path. The summer/winter contrast also becomes much larger.

RAFs can analogously be calculated for other weighting functions [1, 19], as shown in Table 1. The published RAFs for these weightings range from near zero to 2.1, meaning that—at the high end—a 1% reduction in ozone leads to a UV increase of 2.1%. Weightings for which the RAF changes least between summer and winter conditions (e.g. erythema, DNA-damage) would be expected to show the tightest relationship between ozone and UV, as discussed previously [20]. Those compact relationships occur for

weighting functions with a wavelength dependence that is most nearly anticorrelated with ozone's absorption cross section over the critical UVB region.

Note that the action spectrum for erythema adopted in this analysis [28] differs slightly from that used previously [32] by our group, and as previously archived in the NDACC database. As discussed elsewhere [33], the UVI calculated with the later CIE standard is typically ~0.5% larger for small SZAs, increasing with SZA to around 2% larger by SZA = 80°. It was also shown [34] that RAFs calculated from the CIE spectrum are slightly smaller, as would be expected, but the difference is less than 1% for SZA < 60°, increasing to 2% for SZA = 80°.

The action spectrum for DNA damage used in the present analysis is from a parameterisation of Setlow's original data [29], as is used at all NDACC sites [35].

The CIE action spectrum for vitamin D [30] is controversial [31, 36, 37] and includes an arbitrary exponential decay beyond the longest wavelength measured that may not be realistic. Further, a recent study showed more consistent results with observations if the spectrum is moved by 5 nm towards shorter wavelengths [38]. Previously, our group had used a truncated version of the CIE spectrum, falling to zero above 315 nm. That truncation reduces the weighted irradiances for the summer and winter noon spectra shown in Fig. 1 by 4.5% and 14.5%, respectively (and by more at larger SZAs). With that truncated version (UV_{vtd}), the RAF is slightly larger (see Table S1 in Supplementary data). Here we use the full action spectrum published by the CIE [30].

4 Spectrometer data

The UV spectrometers used in this study are part of the international Network for the Detection of Atmospheric Composition Change (NDACC) [3]. High-quality spectral irradiance data that meet their demanding standards [39] are used from four sites where NIWA UV spectrometers have been successfully deployed for 15 years or more. The sites are at low and mid-latitudes in both hemispheres [40] and represent a wide range of altitudes. Details of the sites and data are shown in Table 2.

In normal operation, spectra are logged at 15 min intervals over the 2 h centred on local solar noon, and at 5-degree steps in SZA outside that period up to SZA = 95°. Additionally, a spectrum is logged at midnight.

Each logged spectrum consists of the average of two scans: a reverse scan from 450 to 285 nm and a forward scan back from 285 to 450 nm. Offsets are determined at the turnaround. The scan speed is varied to maintain comparable signal-to-noise statistics at all wavelengths, despite the huge differences in spectral irradiance between those two wavelength limits. The spectral resolution is typically 0.8 nm

Fig. 1 Spectral dependence of (Top panel) UV irradiances at Lauder compared with the ozone absorption cross section [27], (Middle panel) biological weighting functions discussed, and (Bottom panel) spectrally weighted irradiances. Note that curves for weighted irradiance in winter have been scaled by a factor of 10 for clarity, while integrals without scaling are shown for each case in the legend
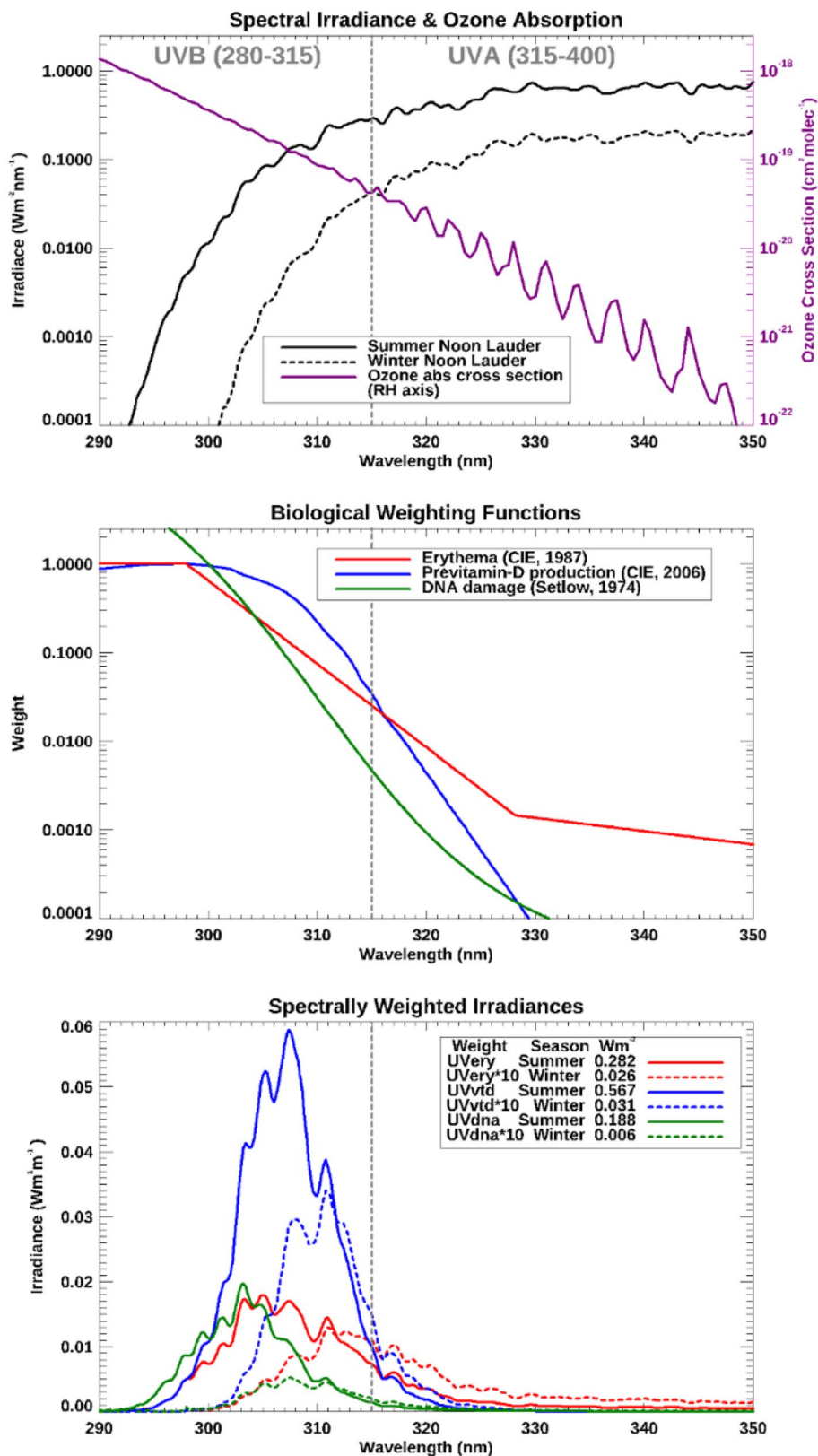
Table 1 RAFs for weighting functions investigated in this study

Weighting	RAF (as calculated for conditions stated below)		
	30°N Jan (290 DU) (Winter)	30°N July (305 DU) (Summer)	Ratio ($\pm$ 0.01) (Summer/Winter)
UVA, Integral 315–400 nm	0.03	0.02	0.67
UVB, Integral 280–315 nm	1.24	0.99	0.80
UVI, Erythema (UV_{Ery}), CIE, 1998	1.13	1.21	1.07
UV_{DNA}, DNA-damaging UV	2.14	2.14	1.00
UV_{VitD}, Previtamin D production, CIE	1.69	1.44	0.85

See Supplementary data for RAFs used in previous studies by our group

Table 2 Measurement sites and Observation periods used

Site	Lat	Long	Alt (km)	Instrument name	Range of Years
Lauder, NZ	– 45.04	168.68	0.4	UV4	2006 to 2021
Alice Springs, Aus	– 23.80	133.87	0.5	UV7	2007 to 2020
Mauna Loa, HI	19.53	– 155.58	3.4	UV3	2005 to 2021
Boulder, CO	40.13	– 105.24	1.7	UV5	2005 to 2021

(fwhm), with sampling at 0.2 nm steps. The entire scan sequence takes approximately 5 min, a period long enough for variable cloud effects to influence the spectra. To recognise cloud-affected data, the variance of UVA irradiances during the scans is determined from the signal produced by a UVA-sensitive diode positioned near the entrance slit.

If the effect of cloud is sufficiently small, the measured spectrum is used to infer total column ozone for a fixed atmospheric profile, using differential absorption at 305 and 340 nm as computed by a simple Radiative Transfer (RT) model [41]. Note that the criteria for this ozone retrieval are just sufficient light levels and low variance in the UVA irradiance; it is not restricted to clear skies or even unobscured sun. Anomalous ozone retrievals can result from a variety of sources.

Regular calibrations are traceable back to NIST giving an overall irradiance uncertainty of 3% (2-sigma), and wavelength accuracy is achieved via correlation alignment with respect to a reference solar extra-terrestrial spectrum. For each logged spectrum the Modelled spectral irradiance is calculated for clear-sky conditions (with no aerosols) at each site using the TUV radiative transfer code [42] with ozone amounts derived from the spectra as described later. The UVA component of each (which is independent of ozone) is then used to calculate the UVA transmission for each spectrum compared with those clear-sky conditions.

Standard outputs for each spectrum are archived and are available from databases maintained by a. NDACC (https://www.ndacc.org) and b. WMO World Ozone and UV Data Center (https://woudc.org/).

As a result of the present analysis, several examples of bad data have been identified. For example, after a temporary

instrument failure at MLO on 14 June 2018, a clock error when data resumed the following day caused ozone retrievals to systematically reduce from 416 near 'noon' down to 298 DU by late afternoon. Similarly, on 28 May 2017, ozone apparently increased from 322 to 365 DU in one morning. Similar outliers were removed on 7 June 2008 and 3 May 2009. While ozone can change over the course of a day, these changes are too large to be realistic and are probably also due to clock errors. According to the NIWA-BS total column ozone global database [43], ozone amounts never exceed 340 DU at this site. The above archives are being updated accordingly. These updates will also implement the current standard CIE weightings for erythema [28] and previtamin D production [30].

The outputs of interest here are.

- Date/time,
- Solar zenith angle (at centre of scan – similar for all wavelengths through symmetry of scan),
- Ozone (retrieved),
- Weighted irradiances (UVA, UVB, UV_{Ery}, UV_{DNA}, UV_{VitD}),
- UVA diode mean and its standard deviation during the scan (for quality control),
- Wavelength shift applied (for quality control) and
- UVA-Transmission. Used for quality control, compared with aerosol-free conditions.

Sample time series of these parameters are shown for the instrument at Lauder in Fig. 2. Also included is the corresponding ozone time series for this site from the NIWA-BS data set [43].
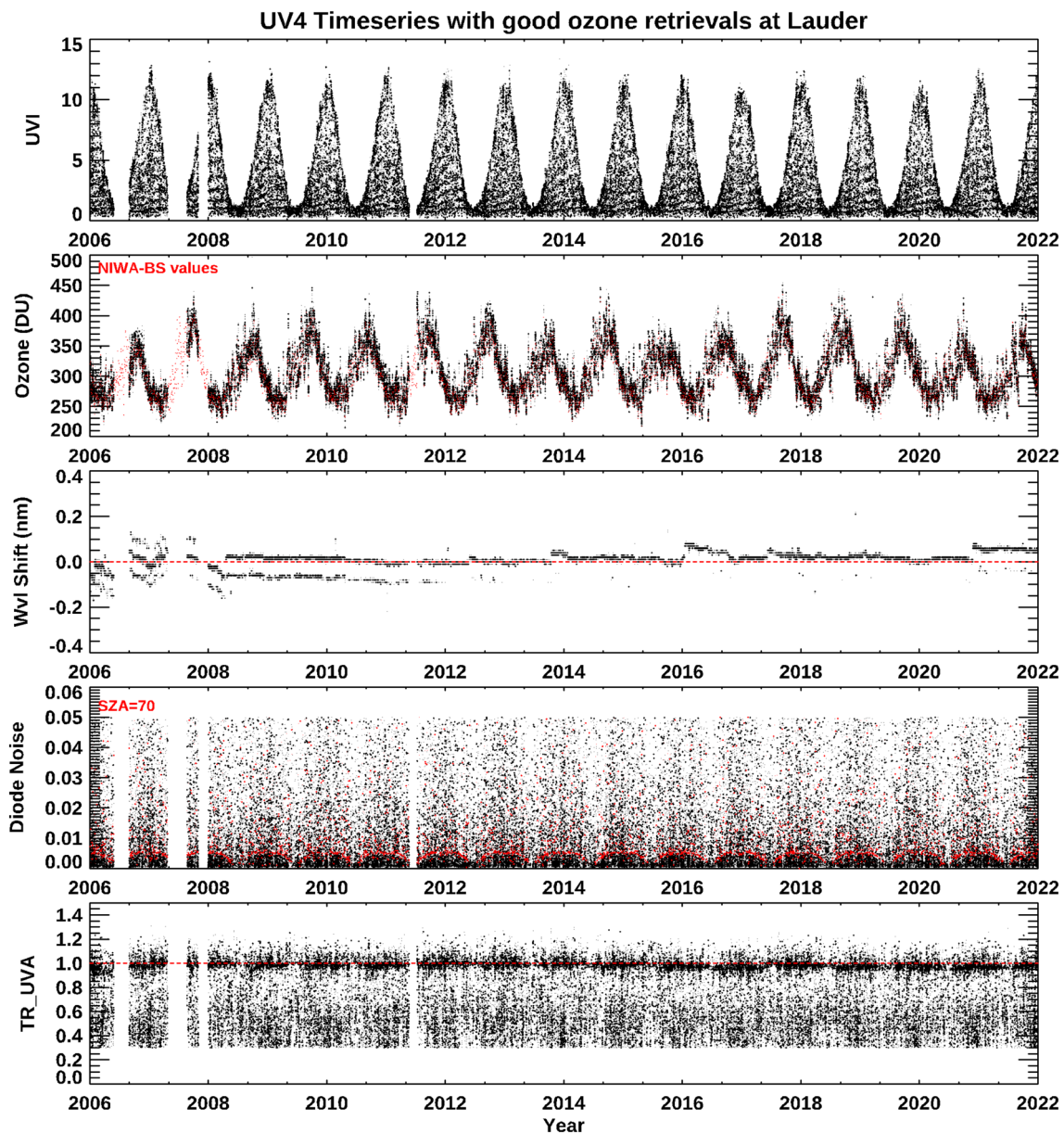
Fig. 2 Times series of several standard processing outputs from the UV4 spectrometer at Lauder. Different wavelength shift groupings are those required to bring forward and reverse scans into alignment with the reference spectrum. The bottom two panels, showing diode noise and UVA transmission, are relative to the mean and clear-sky values, respectively. Note that ozone retrievals are limited to spectra with diode noise less than 5% and UVA transmission greater than 0.3. For other sites see Supplementary data

5 Selection of clear-sky data

Clouds that block the sun can reduce UV irradiances by more than 90 percent, and broken clouds that do not directly block the sun can lead to enhancements greater than 20 percent. To screen against these cloud effects, clear-sky spectra were selected using the statistics of the UVA transmission. Sample histograms for the four sites are shown in Fig. 3.

As in a past study [44], we assume the primary histogram peak corresponds to clear-sky conditions. Here "clear" means free of cloud, whereas the model applies to sky that is both clear and "clean", meaning free of aerosol. Typically the peak in the ratio is in the range 0.90 to 0.98, with lower values at the more urban sites (e.g. Boulder). This shows that reductions in UVA irradiances due to aerosol extinctions are less than 5% at Lauder and MLO, and about 10% at Alice Springs and Boulder.

To avoid effects on irradiances of cloud absorptions or enhancements, we used spectra for which the UVA transmission was within 4 percent of the peaks shown in
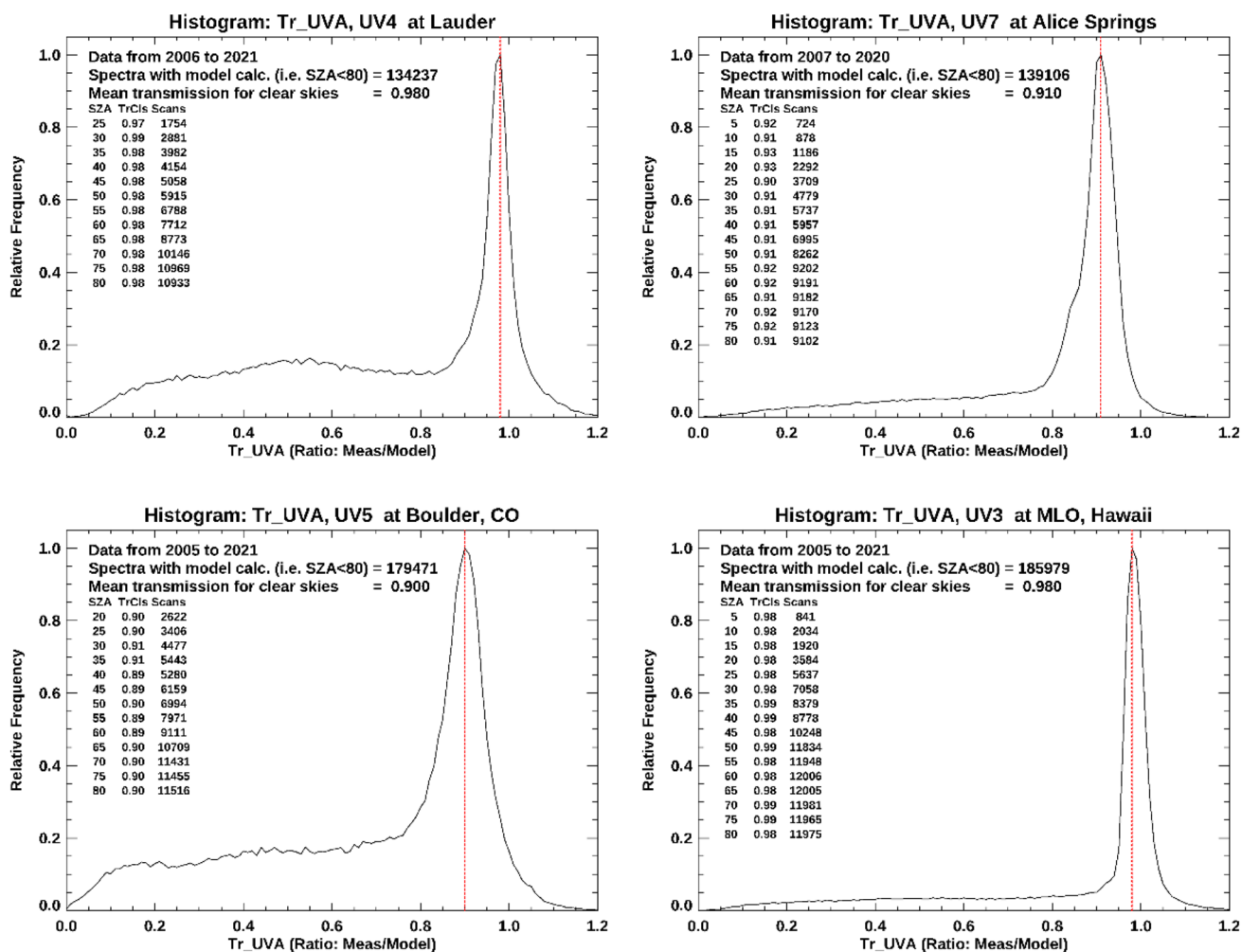
Fig. 3 Histograms of UVA Transmission normalised to the clear-sky peak, for all four sites. Deduced clear-sky transmissions for selected SZAs are also shown. Note the wider range of SZAs available at lower-latitude sites
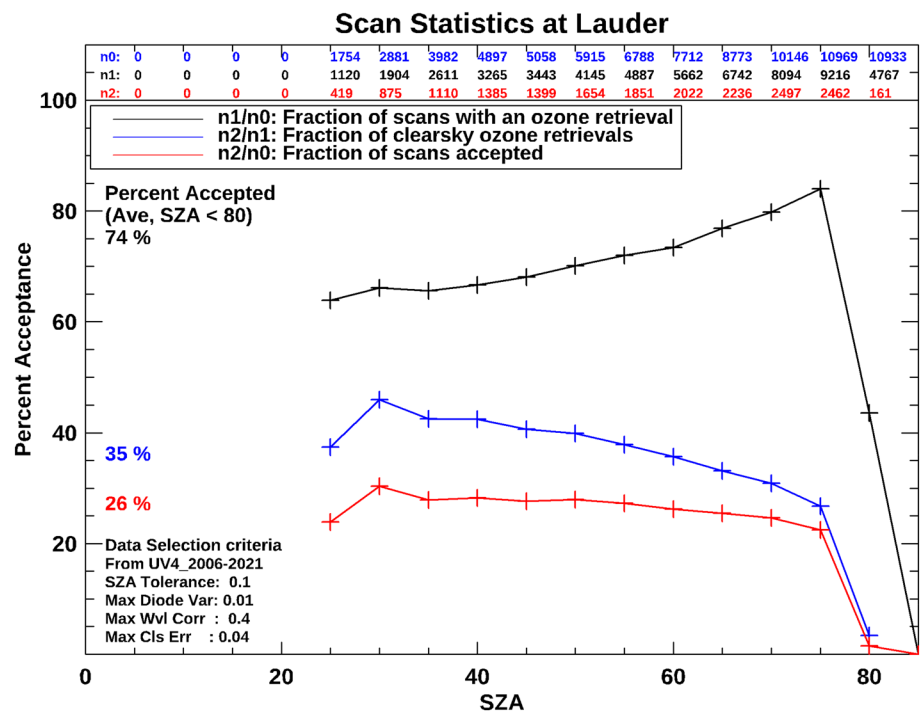
Fig. 3, where a three percent threshold matches the absolute uncertainty of the measurements, and an additional 1 percent allows for numerical errors in calculating the clear-sky UVA transmission. Deduced UVA transmissions for each solar zenith angle considered are shown for each site in the left of each panel in Fig. 3. Any SZA dependencies are small for SZA ≤ 80°. This selection criterion also rejects data for which aerosol extinctions are atypical.

Typically there is a secondary peak near transmission 0.5, but that is less obvious at dry sunny sites, like Alice Springs, or the high-altitude Mauna Loa Observatory where clouds are often below the observatory. We further restricted the data set based on a tighter diode (UVA) noise criterion than was used for screening ozone retrievals. To further block residual cloud effects, we used scans for which the standard deviation of the diode variability during the scan was less than 1% of the mean.

Finally, we allowed only scans for which the wavelength shift to bring the logged spectrum into line with a reference solar spectrum was less than 0.4 nm, as larger shifts can be associated with incorrect correlation alignment. Such errors occasionally occur for spectra measured under changing cloud conditions (so would probably be excluded here anyway).

UV irradiances change rapidly with SZA, especially as the sun approaches the horizon (larger SZAs). A tight SZA selection criterion is therefore required. Because scans are typically logged at 5-degree steps in SZA, we were able to capture most scans with a threshold of ± 0.05°. That tight threshold is required for larger SZA, but by using it we miss some of the midday scans which are logged at time intervals rather than SZA intervals. To mitigate against that we relaxed the criterion to ± 1° for SZA < 40°.

Fig. 4 Data acceptance statistics for Lauder data. The first three lines show n0: the numbers of scans for each solar zenith angle, n1: the number of scans for which ozone retrievals were available and n2: the number of scans accepted for analysis of clear-sky conditions. The black, blue and red curves show n1/n0, n2/n1, and n2/n0 respectively. For other sites see Supplementary data

Scan Statistics at Lauder

n0:	0	0	0	0	1754	2881	3982	4897	5058	5915	6788	7712	8773	10146	10969	10933
n1:	0	0	0	0	1120	1904	2611	3265	3443	4145	4887	5662	6742	8094	9216	4767
n2:	0	0	0	0	419	875	1110	1385	1399	1654	1851	2022	2236	2497	2462	161

n1/n0: Fraction of scans with an ozone retrieval
n2/n1: Fraction of clearsky ozone retrievals
n2/n0: Fraction of scans accepted

Percent Accepted
(Ave, SZA < 80)
74 %

35 %

26 %

Data Selection criteria
From UV4_2006-2021
SZA Tolerance: 0.1
Max Diode Var: 0.01
Max Wvl Corr : 0.4
Max Cls Err   : 0.04

Examples of the percentages of scans remaining for analysis at each SZA are shown in Fig. 4.

There are large site-to-site differences, as well as some SZA dependence, in data acceptance. The black curves show that as the SZA increases, the proportion of scans that include an ozone retrieval also increases (in part because of insufficient resolution in the diode signal used as an ozone acceptance criterion). The blue curves show that the proportion of those that satisfy our clear-sky criteria tends to decrease at larger SZA, particularly for SZA > 75°. The net effect is that only 25% of all scans for SZA < 80° pass the rejection criteria at Lauder. The corresponding fractions for Alice Springs, Mauna Loa and Boulder are 45%, 52% and 22%, respectively. The smaller fraction at Boulder is in part due to noisier data at that site, especially during the period from November 2010 to August 2011 when one of the instrument's cooling units was inoperative. The error manifests itself as departures from expected offset measurements (determined at the wavelength turnaround between the reverse scan and the forward scan), which can affect accuracy at the shortest wavelengths. Steps have been taken to better recognise and correct for this condition, and to update the data archives. Fortunately it is of little consequence in the present study where the only results affected are Boulder's DNA-weighted irradiances at larger SZAs. The smaller number accepted at the largest SZA for which ozone retrievals are available (SZA = 80°) is of little practical consequence because of the low UV irradiances at this SZA.

The total number of scans accepted is large, about 18 and 19 thousand, respectively, at the mid-latitude sites of Lauder and Boulder, and about 37 and 61 thousand, respectively, the low-latitude sites of Alice Springs and Mauna Loa.

6 Ozone retrievals

As noted above, ozone amounts are derived from each spectrum by comparing the ratio of irradiances at 305 and 340 nm with those pre-calculated with a radiative transfer model [41]. In our standard data processing (as archived), ozone retrievals are restricted to scans for which the standard deviation of diode noise is less than 5% of the mean, and the UVA transmission exceeds 0.3. The latter restriction is to avoid overestimations of ozone arising from the increased tropospheric light path due to multiple scattering within and between clouds. In Figs. 5 and 6 we compare retrieved ozone values with those from three other sources: (a) Dobson spectrophotometer data (hereafter abbreviated to "Dobson" data) obtained here from the NDACC data base www.ndacc.org (also available at https://woudc.org/), (b) the NIWA-BS analysis (currently version 3.5.1) available from https://www.bodekerscientific.com/data/total-column-ozone and (c) TEMIS overpass data (OMI version 003 Overpass, available from https://www.temis.nl/protocols/o3col/overpass_omi.php).

Although direct-sun observations using Dobson or Brewer Spectrometers remain the benchmark for ozone

Fig. 5 Ozone time series, and ratios with respect to NIWA-BS values. For other sites, see Supplementary data. Smooth lines are 100-point moving averages
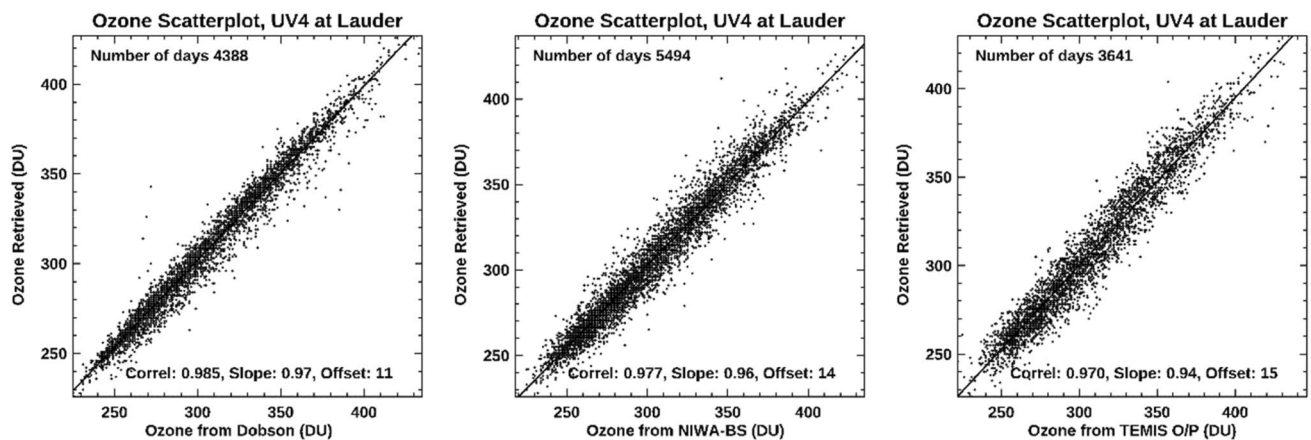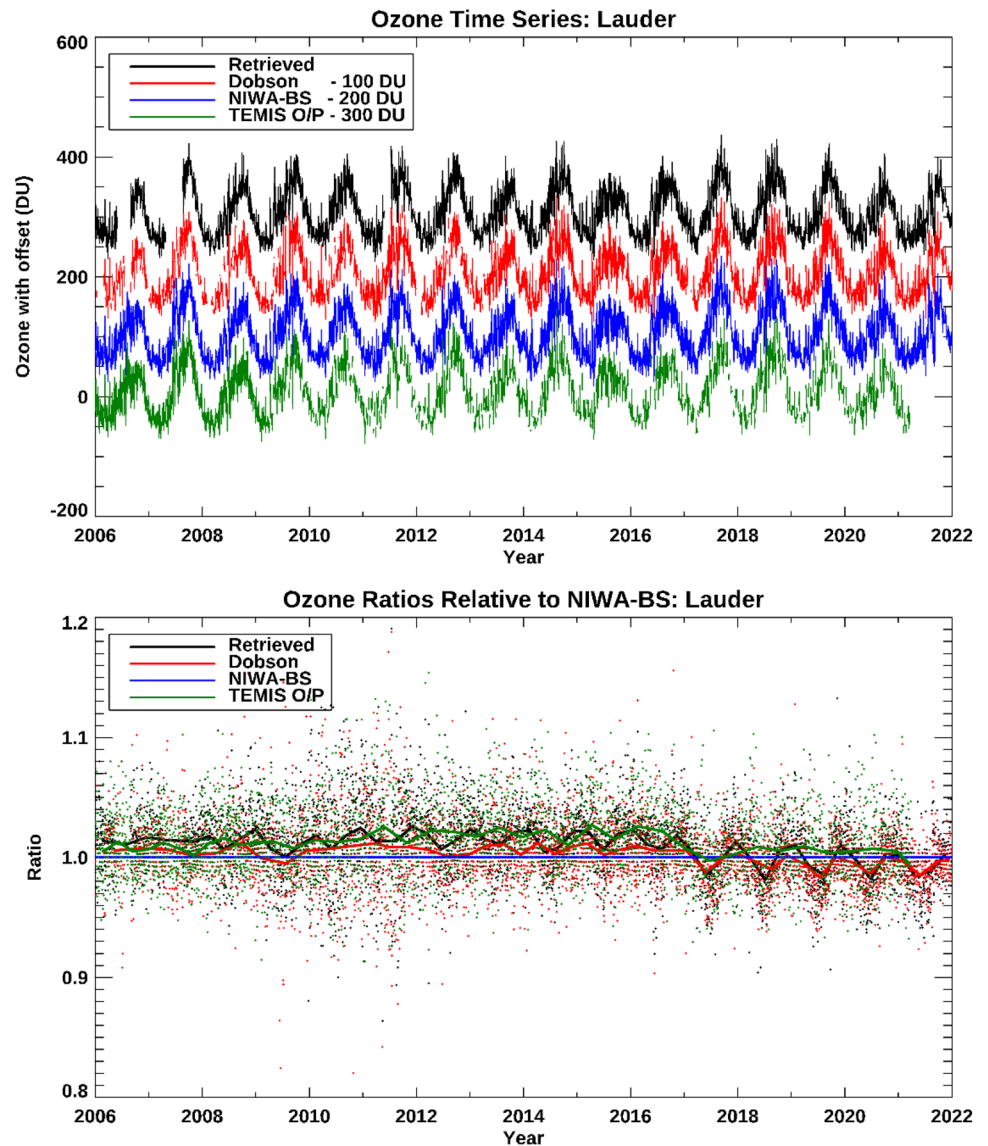

Fig. 6 Ozone comparison between data sources. The label 'correl' is the R^2 correlation coefficient. For other sites, see Supplementary data

Table 3 Correlations between ozone sources at Lauder shown in the upper quadrant

	Retrieved	Dobson	NIWA-BS	TEMIS O/P
Retrieved	1.000	0.985	0.978	0.971
Dobson		1.000	0.975	0.969
NIWA-BS			1.000	0.975
TEMIS O/P				1.000

measurements, such data are not available at all sites so NIWA-BS data are instead used as the reference for comparison in Fig. 5 and Figure S3.

In the great majority of cases, ozone values agree with Dobson data to within the expected 2-sigma uncertainty of ± 3%. There is some seasonality in the standard retrieval relative to the Dobson values, but recent work has shown that the latter in turn have a seasonally varying error similar in magnitude due to seasonal changes in stratospheric temperature [45]. Occasional outliers differ by more than 20%.

Regressions between daily mean ozone retrievals and other sources are shown in Fig. 6. These and Table 3 imply that our retrievals are at least as good as those derived from the overpass data or the NIWA-BS ozone data set.

The agreement between retrieved daily ozone with Dobson values is similar to that with NIWA-BS ozone and is slightly better than with the TEMIS product (where data frequency also declines over the study period). Unfortunately, no Dobson data are available at Alice Springs. The nearest active Dobson site, Darwin (12.5°S), is 1300 km north.

In view of recent differences identified between the NIWA-BS ozone series and other ozone data [46],[1] it is perhaps worth noting that any systematic differences over time compared with Dobson values at these sites are less than ± 3%, which is close to the standard uncertainty of the Dobson instruments [47, 48]. A more recent study suggests the absolute accuracy of Dobson data may be closer to 2% (2-sigma), much of which arises because no account is taken of the temperature dependence discussed above [45]. Table 3 shows that at Lauder the retrieved ozone correlates more strongly with the Dobson ozone values ($r^2 = 0.985$) than with the NIWA-BS values ($r^2 = 0.978$), though the number

of days available for comparison is smaller (as shown in Fig. 6). Outliers between Dobson and NIWA-BS ozone values are larger than between our retrieved ozone and NIWA-BS values, sometimes exceeding 50 DU.

With our standard data rejection criteria, retrieved ozone amounts can still occasionally be too high under cloudy conditions. To avoid those outliers, tighter rejection criteria are needed (e.g. diode noise standard deviation less than 1% and UVA transmission greater than 90%). When these are applied, a weak dependence on SZA can be seen, though previous work has shown that ozone retrievals by this method agree well with those from co-located Dobson instruments, with differences typically less than 10 DU for SZA < 70° [41]. For larger SZAs, systematic differences can exceed 20 DU. Although it will be of little consequence in the present study, where we compare results from the same SZA, we nevertheless apply corrections by investigating the SZA dependence of retrievals, relative to the retrieval for SZA = 30°. That error analysis is limited to summer months when ozone variability is small and when observations are available over a wide range of SZAs. Results for Lauder, are shown in Fig. 7.

Corrections are typically less than 2%, and any differences between the data and the quadratic fitting function are less than 1%. Corrections with similar uncertainties were derived for other sites (see Supplementary data).

The accuracy of ozone retrievals—before and after these SZA corrections—was assessed by their correlation with corresponding daily ozone measurements archived in the NIWA-BS ozone analysis (version 3.5.1). Results are shown in Fig. 8, which shows that the agreement is satisfactory, with overall correlations exceeding 0.98, though occasional outliers sometimes still differ by more than 30 DU.

Note that the overall fit, expressed as

$$O_{3retrieved} = 11 + 0.981 O_{3NIWA-BS}$$

in DU, gives the offset of 11 DU at the origin of the x-axis $O_{3NIWA-BS} = 0$ DU. Over the range 215–430 DU, the mean offsets $(O_{3retrieved} - O_{3NIWA-BS})$ are smaller, ranging from 4 to 8 DU.

Figure 8 shows that there is some residual SZA dependence in the ozone retrievals. However, the effect is small. The lower correlation at SZA = 25° arises because of the smaller number of scans available and the smaller range of ozone that occurs in the summer period when this SZA is reached, making the deduced gradient and offset (again, at the origin) for that SZA less certain. The agreement remains similar for SZA from 30° to 70°, but becomes larger for SZA > 70°.

In the main analysis here, we use ozone values retrieved from the spectrometers. Although they may include a bias of up to 2 or 3 percent, they are the most complete data set

---

[1] Version 3.5.1 of the NIWA-BS database used overpass data for calculating the bias corrections using data files that were not intended by the NASA ozone processing team for public release. This resulted in biases of up to 6 DU for different periods of the record from 1978 to 2019. However, since 2005, the bias was close to zero. As such, while this version of database as a whole is unsuitable for trend analysis, the data from 2005 onwards remain valid for process studies (personal communication, Greg Bodeker, Bodeker Scientific, 13 June 2022). For more information, see https://storage.bodekerscientific.com/Bodeker%20Scientific%20TCO%20V3.4.x%20and%20V3.5.x%20differences.pdf.
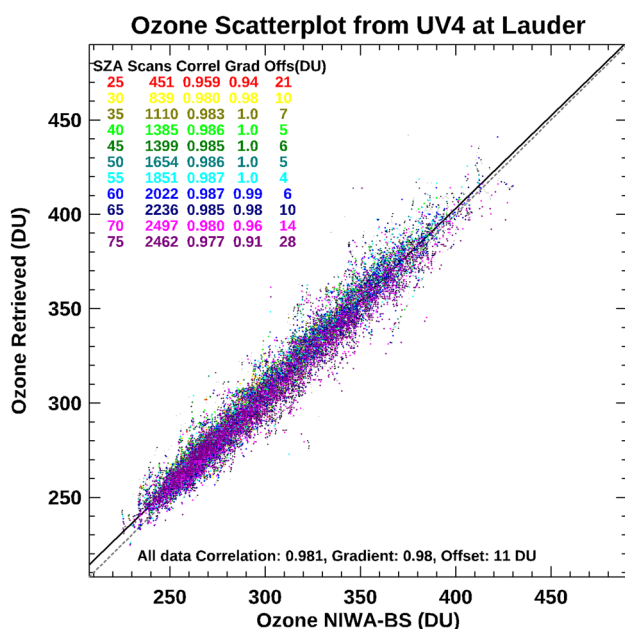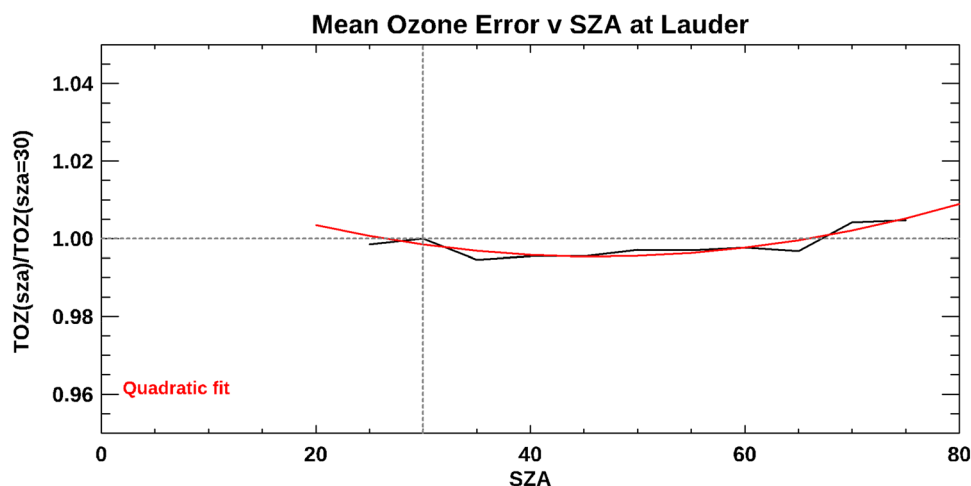
Fig. 8 Scatterplot of derived ozone as a function of ozone from the
NIWA-BS analysis at Lauder (for other sites, see Supplementary
data)

available and the only one which captures diurnal changes
in ozone, which can be much larger than that bias (see
Fig. 5). They also avoid errors from interpolating satellite
data with footprints of tens of kilometres (the footprint of
the OMI instrument for example is 13×24 km at best),
especially in the case of Mauna Loa where the mountain
observatory is far above the mean terrain height. How-
ever, in Supplementary data we compare the final results
with those obtained from the NIWA-BS product, which
is the most complete and shows closest agreement with
Dobson values. It has been used widely in previous WMO
Ozone Assessments as well as in our own studies (e.g. Ref
[49]) and utilises ozone measurements from all available

satellite data products (including TEMIS OMI data) [50].
Accuracy for trend analysis is assured (though see ear-
lier footnote regarding v3.5.1) by normalising to ground
based data. The time series for each location in Table 2
are obtained by spatial interpolation from the $1.25° $ lon-
gitude $\times 1.0°$ latitude grid. In the supplementary data, the
final result is also shown using TEMIS ozone values.

7 Seasonal variabilities

At mid-latitudes, there are large seasonal variations in
ozone, which are responsible for large seasonal variations
in UV irradiances for a given SZA. Plots of these sea-
sonal variations clearly show their strong anticorrelation,
as illustrated in Fig. 9 for the UV Index at Lauder. Sea-
sonal changes in UVI are larger at smaller SZAs, but data
are not available for all seasons at this site for SZA < 70°.
For a given SZA, the lowest ozone amounts and highest
UV irradiances occur in autumn (March–April at Lauder),
when the mean UVI can exceed that in spring by more than
50%. However, there are also large day-to-day variabilities,
and peak differences can approach 100%. That variabil-
ity is larger than one would estimate from application of
Eq. 1. The RAF for erythema of 1.2 implies that for 1%
reduction in ozone, the UVI increases by 1.2%. But for
seasonal ozone reductions, which can be as large as 50%,
the implied increase in UVI exceeds 100% according to
Eq. 2.

From a human health perspective, it is fortunate that the
UVI is lower in spring than in autumn for the same SZA
because pale skin (Fitzpatrick types I to III) [51] has lit-
tle adaptation to UV damage in spring, whereas by autumn
protective skin pigmentation has usually increased. The
seasonal variability is less pronounced at low latitudes (see
Supplementary Data), but the anticorrelation remains clear.

Fig. 9 Seasonal variability of ozone and UVI at Lauder. Coloured dots show UVI relative to the mean for each SZA. The joined lines show UV and retrieved ozone relative to their respective means for SZA = 75°. For other sites see Supplementary data
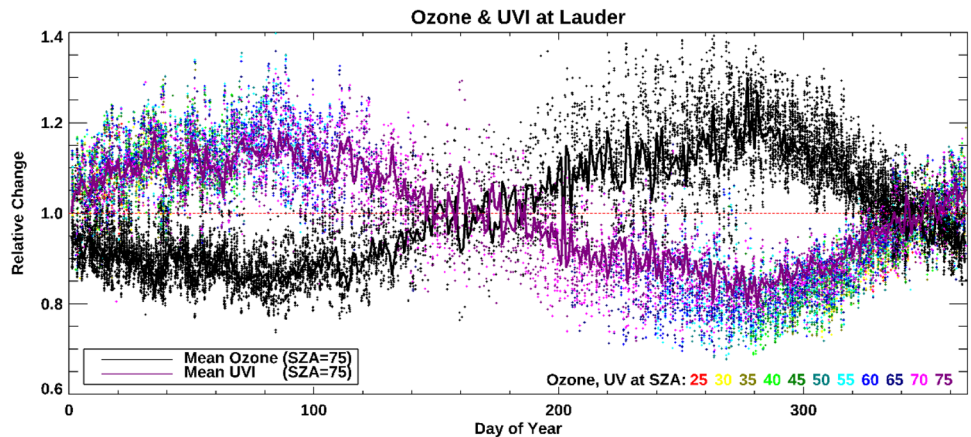
8 Comparing UVI between sites

In a past study we had shown that, for the same SZA and ozone amounts, the peak UVI for these sites is largest at MLO and smallest at Boulder, with differences being attributable to altitude, aerosol optical depth and Sun–Earth separation in summer [44]. But those maxima in peak UVI include possible cloud enhancement events, which may differ between sites depending on the cloud characteristics.

In Fig. 10 we compare the UVI between the four sites as a function of ozone. To facilitate the comparison between sites, only data for SZA = 25° or greater are displayed (also in Fig. 11), because there is limited data coverage for smaller SZAs at the highest-latitude site (Lauder). At the low-latitude Mauna Loa and Alice Springs sites, where the minimum SZA is much less than at Lauder, the UVI can far exceed the data points displayed in these plots. However, despite Boulder's higher altitude, and its minimum SZA being 5° smaller than at Lauder, its UVI maxima are similar to those at Lauder. Absolute and clear-sky maximum UVI values are therefore provided in the legend of Fig. 10, along with a "reference" value derived from the measurements for SZA = 30°, ozone = 300 DU, and for 1 AU Earth–Sun separation. These reference values provide a convenient comparison point between sites. Data are shown for 5-degree steps in SZA between 25° and 80°. To strengthen the relationship between UVI and ozone, all UVI values have been corrected to a Sun–Earth separation of 1 AU (which reduces peak summer values in the Southern Hemisphere by around 3% and increases those in the Northern Hemisphere by a similar amount).

Note the lower ozone amounts and smaller range of ozone values at the more tropical sites. As expected, the highest UV irradiances occurred in all cases for the lowest SZAs, corresponding to the summer season at each site. Note also that summer ozone amounts—as seen for the low SZAs—tend to be larger in the NH, especially at mid-latitudes. As noted previously [52], these lower summer ozone amounts

contribute significantly to the higher peak UVI seen at Lauder compared with Boulder. Despite Lauder being 5 degrees of latitude further from the equator, and nearly 1.5 km lower in altitude, the peak UVI at Lauder exceeds that at Boulder by approximately 10%. As expected, the reference values (for 1 AU) are more similar.

To facilitate comparison between sites for their common range of SZAs, the y-axes in Fig. 10 are all truncated to 16 to include the highest value observed for SZA = 25°. Larger values can occur for smaller SZA at the tropical sites, as noted in the legend. The largest UVI for a given SZA occurs at the high-altitude MLO site. Although its distance from the equator is similar, the peak UVI at Alice Springs is much lower. At all sites the minimum SZA is less than 25 degrees, and for the lowest-latitude site (MLO), the sun is at times directly overhead. Consequently, the absolute maximum UVI is larger than shown for these fixed SZAs. For example, at Mauna Loa Observatory, the maximum clear-sky UVI is 17.7, and the absolute maximum is 21.2, about 20% greater. For other sites, the peak values exceed the clear-sky maxima by less than 10%. The larger enhancement at MLO may be attributable to frequent occurrence of clouds below the altitude of the observatory which increases the effective surface albedo [44].

For fixed SZA and ozone (e.g. SZA = 30°, total ozone = 300 DU), the UVI (corrected to 1 AU Sun–Earth separation) ranges from 8.35 at Alice Springs up to 10.3 at MLO, as shown in Table 4. Assuming differences in the ozone profile are not important, this implies that, after allowing for the calculated altitude differences between sites, aerosol extinctions cause only small reductions in UVI at Lauder and MLO, but reduce the UVI at Alice Springs and Boulder by 6% and 9%, respectively (a smaller difference compared with other US sites than deduced from our previous study that investigated peak UVI values that include cloud enhancements) [52]. Note that the ratios shown in Table 4 exclude most data with enhancements because they do not meet our data inclusion criteria.

Fig. 10 Comparing UVI as a function of ozone between the four sites considered (see Tables 2 and 4 for site details). The left plots are mid-latitude sites, and right plots are low-latitude sites, with SH and NH at top and bottom, respectively. NPTS is the number of scans meeting all selection criteria. For other weightings, see Supplementary data
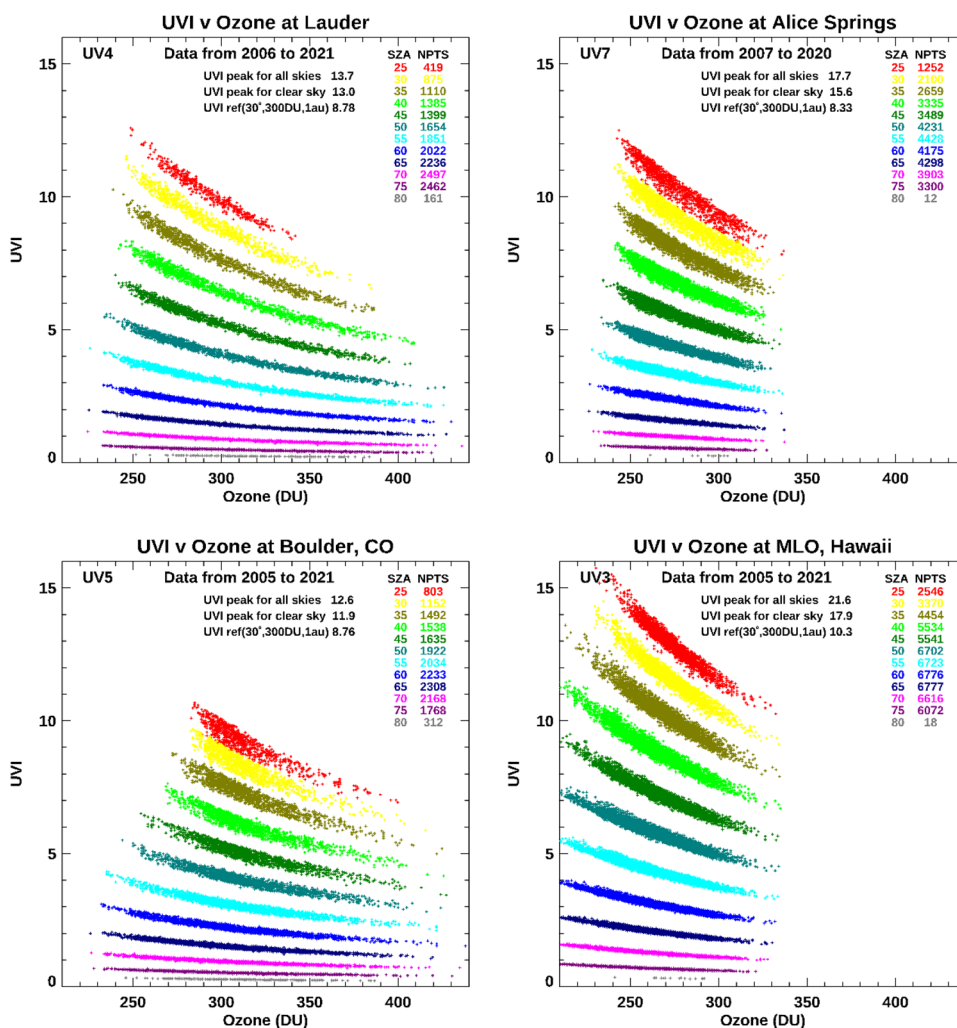
The larger noise in data from Boulder mentioned previously has little effect on UVI or most other weightings. Its effects are most apparent in corresponding plots of DNA-weighted UV, for SZAs $\geq 70°$ (see Supplementary data). However, only a relatively small number of scans is affected ($< 1\%$ for SZA $< 80°$), and tests using different data periods show that it has insignificant effects on the deduced RAFs.

9 UVI ozone dependence between sites

The dependence of UVI on ozone is shown for several SZA at four sites in Fig. 11.

Seasonal changes in ozone are larger at the middle-latitude sites. For example, at Lauder the minimum ozone values are approximately 50% of the maxima, and the corresponding largest UVIs exceed the smallest by more than a factor of 2. The UVI dependence on ozone is similar at each site, and is well represented by the published RAFs calculated using the TUV radiative transfer model (Table 1).

For SZAs less than 75°, the RAFs calculated from the data are within 10% of the calculated values. But for larger SZAs calculated RAFs are lower, as expected [20].

10 Ozone dependencies for other weightings

Similarly, we use these seasonal and day-to-day differences in ozone to illustrate the dependence of other UV irradiance weightings on ozone for several SZAs. Example plots using Lauder data for UV_{DNA}, UV_{VitD}, UVB and UVA are shown in Fig. 12.

The number of outliers is a very small fraction of the thousands of data points displayed in each panel of Figs. 10 and 11. The tightest relationship is seen for DNA-weighted UV, for which the wavelength dependence of the action spectrum through the UVB region most closely correlates with the absorption cross section for ozone (as shown in Fig. 1), with both following an exponential decay

Fig. 11 Same data as shown in Fig. 10, except with UVI and ozone plotted as ratios relative to the ozone mean for each SZA and its associated UVI value. The black curve is the power law with RAF = 1.13. For other weightings, see Supplementary data
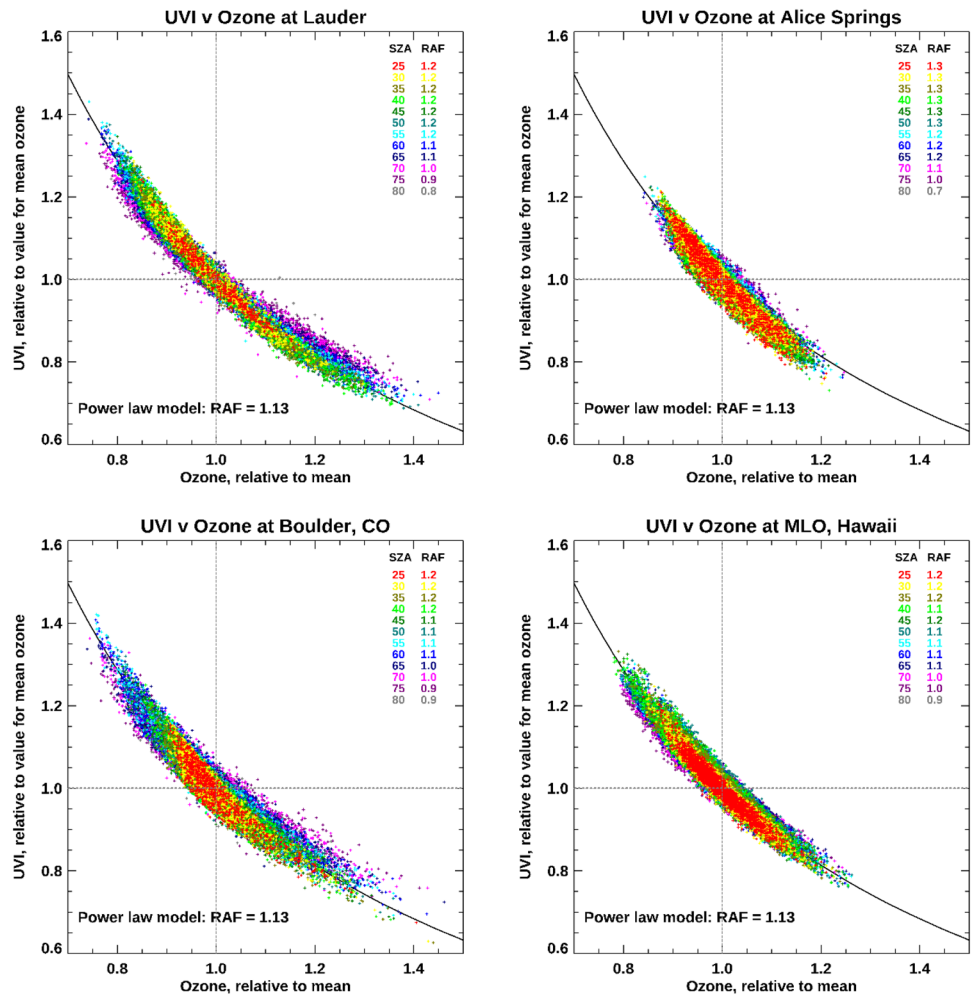

Table 4 Calculated and measured UVI reference values at each site

Site	Alt(m)	UVI Calc	UVI Meas	Meas/Calc
Lauder NZ	370	8.7	8.89	1.02
Alice Spr. AU	500	8.8	8.31	0.94
Boulder, CO	1700	9.3	8.78	0.92
MLO, HI	3400	10.1	10.4	1.03

The calculations here used the TUV radiative transfer model [42] for aerosol-free clear skies assuming a surface albedo of 0.05. Both measured and model values assume an Earth–Sun separation of 1 AU. Also shown are the ratios of measured to calculated values

fairly well over the relevant spectral range. In this case, the measurements for all SZAs faithfully follow those predicted by the published RAF of 2.2. The spread increases as the weighting functions depart from exponential decay in the UVB region. For UVA, where the weighting is zero throughout the UVB region, no significant signal is apparent, and the spread of results corresponds to the clear-sky data selection criterion of $\pm 4\%$.

As expected, seasonal differences in UV are larger for weighting functions with larger RAFs. For DNA-weighted UV, the increase is a factor of three, and for UV_{VitD} it is more than a factor of two.

For DNA-weighted UV, the ozone relationship is more compact than for UVI. However, in cases where the action spectrum fall-off with wavelength is far from exponential (e.g. UVB), there is a large spread of gradients between SZA's, highlighting an important limitation of applying RAFs without taking account of their dependencies on SZA and ozone.

11 RAF comparison

As noted earlier, the RAF for any UV weighting is given by the negative slope of the regression line for log(UV) plotted as a function of log(ozone). In Fig. 13, we show the thus-calculated variability of RAFs between sites for each weighting considered. The calculations use the same data selection criteria used previously to remove cloud effects.

Fig. 12 Relative change in UV as a function of the relative change in ozone at Lauder for several weightings. For other sites see Supplementary data
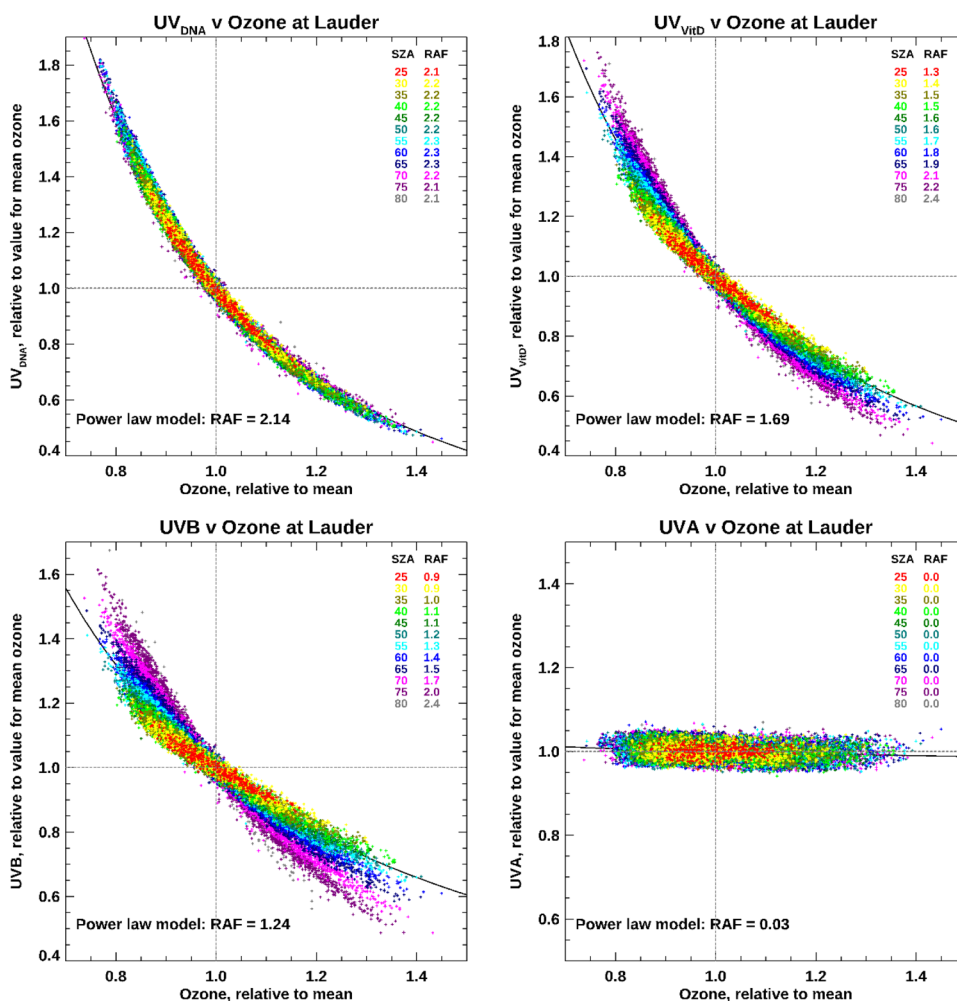
Namely, data are included only if the UVA is within 4% of the deduced clear-sky values, and the diode noise standard deviation is less than 1%.

Despite the tight data selection criteria, the number of data points remaining is still large, so the 2-sigma uncertainty limit in fitting, denoted by the dashed curves, is rather small. Uncertainties are larger at the smallest SZA where there are fewer data points covering only a small seasonal range, and also at the largest SZA where signals become small. For each site, the minimum SZA is limited by the latitude. RAFs for overhead sun are possible only at the tropical Mauna Loa Observatory site, but even there no RAF is calculated for overhead sun because the number of scans satisfying our rejection criteria was too small for inclusion.

In all cases, the RAFs measured at Lauder show excellent agreement with those previously calculated for summer and winter (Table 1). RAFs at other sites show a similar SZA dependence, but there are slight offsets which sometimes exceed the fitting error bars. The variability between sites in RAFs for UVA—which is close to zero because it is essentially independent of ozone—suggests that other factors, such as seasonal changes in aerosol optical depth, can lead to uncertainties of approximately ± 0.1 in the RAF deduced from measurements. For most weightings, the RAFs agree within that limit. However, there is a tendency for lower RAFs for UVB and UV_{VitD} at the high altitude Mauna Loa Observatory (blue curves). As noted in past work [20], RAFs show some dependence on ozone, so slight differences between sites are expected. For example, the slightly larger observed RAFs for UVI at Alice Springs (red curve) could be explained by the lower ozone amounts there [21], or might be due to wavelength-dependent aerosol extinctions. In the case of MLO, which has similarly low ozone amounts and variability, there may be additional imperfectly modelled compensating factors (e.g., surface albedo effects, or altitude effects). In any case, the differences are small. RAFs for erythema measured at Mauna Loa Observatory are closer to calculated values than previously reported from a single year of data [23], though differences are not statistically significant.

Considering DNA-weighted UV, for which the wavelength dependence of the action spectrum is well

Fig. 13 Calculated RAFs as a function of SZA for (top to bottom) UVA, UVB, UVI, UV$_{DNA}$ and UV$_{VitD.}$ for cloud-free conditions (i.e. UVA transmission within 4% of clear-sky values, and diode noise less than 1%). Results for different sites are denoted by different-coloured curves. Dashed curves are 2-sigma limits to the RAF fit. Large grey symbols are calculated RAFs from Table 1
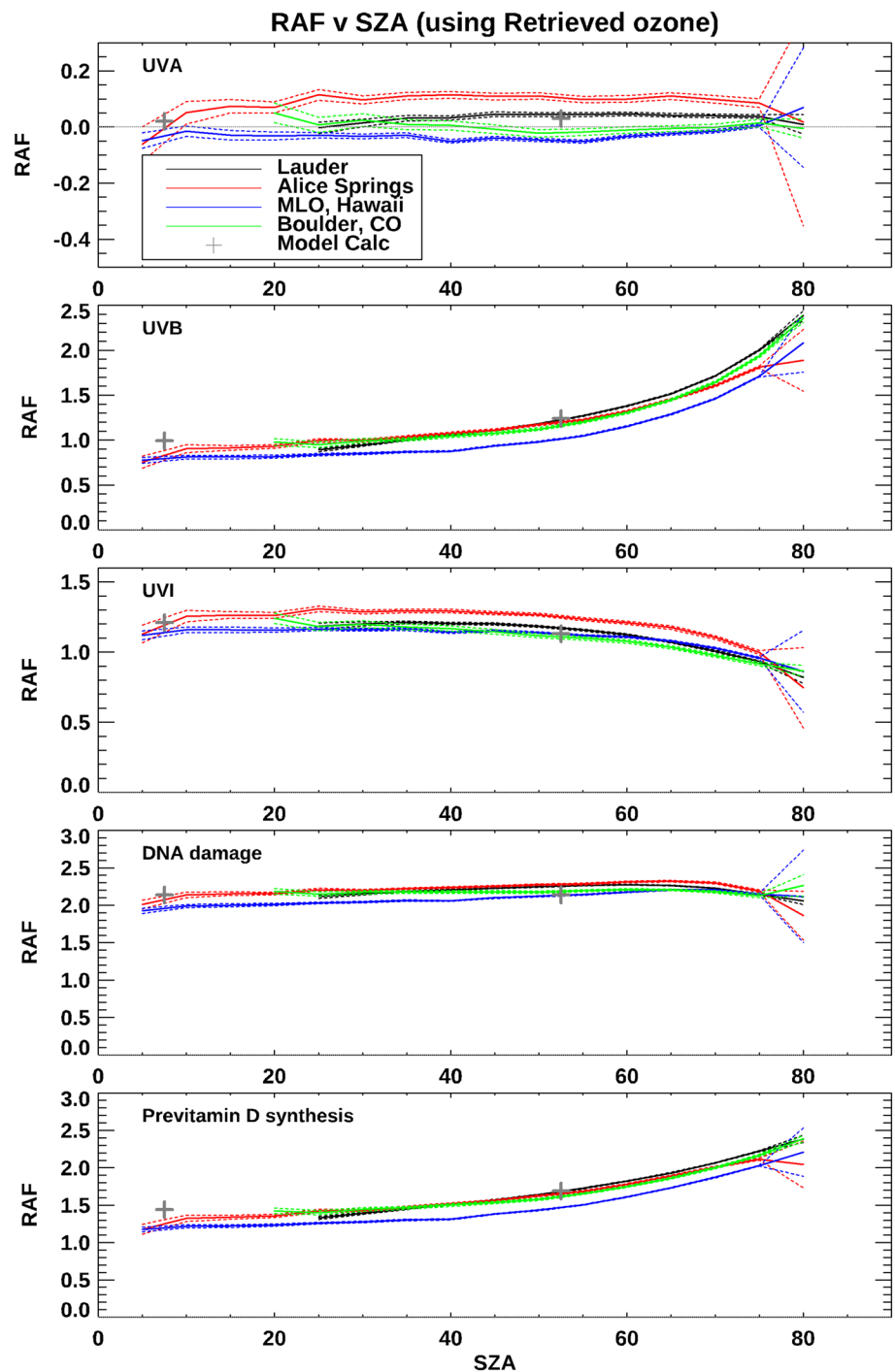
described by an exponential decay, the RAFs show little SZA dependence. For the weighting functions that drop off increasingly more steeply with wavelength, or do not extend into the UVA region (i.e. UVB), the RAFs increase with increasing SZA. Conversely, for UVI (erythema), where the weighting function drops off less steeply in the UVA region, RAFs decrease with increasing SZA. These findings are in line with previous calculations [20].

This remarkable agreement between modelled and measured RAFs for all weightings and sites raises the question of whether it is influenced by any circularity in the argument. There are two potential circularities. The first is from the clear-sky selection method that requires UVA irradiances from the same spectra analysed to be within 4% of the statistically derived clear-sky values. It would perhaps be preferable to select clear-sky data from some other means, but

there is not a suitable alternative that is available at all sites. The second is from using ozone values derived from the same spectra. These considerations are discussed in the Supplementary data where it is shown that the results in Fig. 13 are largely independent of both.

Interestingly, the tendency for RAFs to be slightly lower at MLO (Fig. 13) than for other sites is not replicated when using the NIWA-BS ozone data (Figure S18), despite their larger random errors. The reasons for this are not fully understood. We note that our ozone retrievals at this site were lower than from other ozone data sources. The slightly lower RAFs may be due to an ozone offset, or they may be a consequence of the unique geometry at this site, where the tops of cloud decks are frequently seen below the observatory. In such cases, the surface albedo will be much higher than the value of 0.02 that was assumed in the radiative transfer model used to produce the ozone lookup table. If these underlying cloud events are correlated with ozone, then the deduced RAFs could be affected. In turn this would also imply that the retrieval method will be less accurate during snow cover, unless the lookup table is modified accordingly for such conditions. Investigations are continuing.

12 Conclusions

Data screening to remove cloud effects leaves between 20 and 50% of the data, depending on the site's cloudiness. The screening also removes atypical aerosol effects, the mean values of which are deduced from histograms of UVA transmission. Mean aerosol effects are small at all four NDACC sites. Their mean extinction losses range from less than 5% at Lauder and Mauna Loa to approximately 10% at Alice Springs and Boulder.

Ozone amounts derived from the spectral measurements are in good agreement with those from time series extracted for each site from other sources, including the NIWA-BS global analysis, TEMIS satellite OMI instrument overpass data and (where available) Dobson measurements.

Seasonal variabilities in ozone can double the clear-sky UVI for a given SZA. Changes are even larger for the steeper DNA weighting, where seasonal differences in UV_{DNA} at the same SZA can exceed a factor of four. For UVB and UV_{VitD}, seasonal changes can exceed a factor of three, but that seasonal change depends strongly on the SZA, with the largest changes at large SZAs where UVI is small.

RAFs deduced from these measurements agree well with calculated values. For weighting functions like DNA that are strongly correlated with ozone absorption through the UVB region, correlations are tightest, and the RAFs are approximately independent of SZA.

The RAF for erythemally weighted UV and the widely used UVI is particularly useful because it shows only small variations with SZA. For weighting functions (e.g. UVB) that are poorly correlated with the ozone absorption cross section (i.e. exponential decay over the UVB region), the concept of RAF has limited applicability.

Results for all weighting functions are similar at all four sites and indicate a similar SZA dependence within an RAF uncertainty limit of approximately ± 0.1 when using ozone measurements derived from the spectra. However, at the high mountain Mauna Loa observatory, where the cloud tops are frequently below the observatory, deduced RAFs tend to be slightly lower than at other sites.

Similar RAFs and SZA dependencies are found for all sites—including Mauna Loa—if ozone values from the NIWA-BS ozone analysis are used, or if the clear-sky condition is relaxed (though in this latter case, error bars increase).

The near constancy of RAFs for some biological weighting (UV_{bio}, e.g. erythema and DNA damage) means that the same percentage change, for a given percentage change in ozone, is applicable to instantaneous UV_{bio} irradiances as well as to doses integrated over hours, days, seasons, or even multiple years. This conveniently allows rapid preliminary estimation of relative changes in UV_{bio}, bypassing the need for full action spectra and radiative transfer modelling (though of course with some loss of accuracy).

That the expected RAF relationship of Eq. 3 can be derived objectively from high-quality spectral data at all four sites confirms the large UV variations, which are mostly seasonal, but may also have strong variability on other time scales. The seasonality generally increases with latitude. The strength of the relationship under clear skies for relatively unpolluted sites means that it could be used as an early check on the interpretation of anomalous UV measurements.

Declarations

Conflict of interest The authors declare no financial interest beyond their benefits from employment.

References

1. Madronich, S., McKenzie, R. L., Björn, L. O., & Caldwell, M. M. (1998). Changes in biologically-active ultraviolet radiation reaching the Earth's surface. *Journal of Photochemistry and Photobiology B: Biology, 46*(1), 5–19. https://doi.org/10.1016/S1011-1344(98)00182-1

2. UNEP (1998). *Environmental effects of ozone depletion: 1998 assessment*, [J. C. v. d. Leun, X. Tang, & M. Tevin (Eds.)]. United Nations Environment Programme, Vol. ISBN 92–807–1724–3. UNEP, Nairobi.

3. De Mazière, M., Thompson, A. M., Kurylo, M. J., Wild, J., Bernhard, G., Blumenstock, T., Braathen, G., Hannigan, J., Lambert, J.-C., Leblanc, T., McGee, T. J., Nedoluha, G., Petropavlovskikh, I., Seckmeyer, G., Simon, P. C., Steinbrecht, W., & Strahan, S. (2018). The Network for the Detection of Atmospheric Composition Change (NDACC): History, status and perspectives. *Atmospheric Chemistry and Physics, 18*(7), 4935–4964. https://doi.org/10.5194/acp-18-4935-2018

4. WHO (2002). *Global solar UV Index: A practical guide*. Geneva: World Health Organisation (WHO), World Meteorological Organisation (WMO), United Nations Environment Program (UNEP), and International Commission on Non-Ionising Radiation Protection (ICNRP), https://apps.who.int/iris/handle/10665/42459.

5. Latarjet, R. (1935). Influences des variations de l'ozone atmospherique sur l'activite biologique du raynnoment solaire. *Rev. Opt. Theor. Instrum., 14*, 398–414.

6. Coblentz, W. W., Stair, R., & Hogue, J. M. (1931). The spectral erythemic reaction of the human skin to ultraviolet radiation. *PNAS, Proceedings of the National Academy of Sciences, USA, 17*, 410–405.

7. National Research Council. (1975). *Environmental Impact of Stratospheric Flight*. National Academies Press.

8. Molina, M. J., & Rowland, F. S. (1974). Stratospheric sink for chlorofluoromethanes: Chlorine atom-catalysed destruction of ozone. *Nature, 249*(5460), 810–812. https://doi.org/10.1038/249810a0

9. Urbach, F., Davies, R. E., & Berger, E. (1975). Part 1: Ultraviolet Radiation Effects. In D. S. Nachtwey, M. M. Caldwell, & H. R. Biggs (Eds.), *CIAP Monograph 5: Impacts of Climate Change, DOT-TST-75–55*. Washington, DC: U.S. Department of Transportation, Climatic Impact Assessment Program (CIAP)

10. Rundel, R. D., & Nachtwey, D. S. (1978). Skin cancer and ultraviolet radiation. *Photochemistry and Photobiology, 28*(3), 345–356. https://doi.org/10.1111/j.1751-1097.1978.tb07717.x

11. Gerstl, S. A. W., Zardecki, A., & Wiser, H. L. (1981). Biologically damaging radiation amplified by ozone depletions. *Nature, 294*(5839), 352–354. https://doi.org/10.1038/294352a0

12. Stordal, F., Hov, & I. S. A. Isaksen (1982). The effect of perturbation of the total ozone column due to CFC on the spectral distribution of UV fluxes and the damaging UV doses at the ocean surface: A model study. In J. Calkins (Ed.), *The Role of Solar Ultraviolet Radiation in Marine Ecosystems*. New York: Plenum

13. Farman, J. C., Gardiner, B. G., & Shanklin, J. D. (1985). Large losses of total ozone in Antarctica reveal seasonal ClOx/NOx interaction. *Nature, 315*(6016), 207–210. https://doi.org/10.1038/315207a0

14. Madronich, S. (1993). UV radiation in the natural and perturbed atmosphere. In M. Tevini (Ed.), *UV-B Radiation and Ozone Depletion: Effects on Humans, Animals, Plants, Microorganisms, and Materials* (pp. 17–69). Lewis Publishers.

15. Madronich, S. (1993). The atmosphere and UV-B radiation at ground level. In A. R. Young, L. O. Bjorn, J. Moan, & W. Nultsch (Eds.), *Environmental UV Photobiology* (pp. 1–39). Plenum Press.

16. Brasseur, G., Boville, B. W., Bruhl, C., Caldwell, M. M., Connell, P. S., DeRudder, A., Douglass, A., Dymnikov, V., Fisher, D. A., Frederick, J. F., Garcia, R., Granier, C., Hennig, R., Hitchman, M., Isaksen, I., Jackman, C. H., Ko, M., Madronich, S., . . . Zadarozhny, A. (1989). Theoretical predictions. In *Scientific Assessment of Ozone Depletion*, *Global Ozone Reasearch and Monitoring Project, Report no. 20*, 282–399: WMO https://csl.noaa.gov/assessments/ozone/1989/report.html

17. Booth, C. R., & Madronich, S. (1994). Radiation amplification factors: Improved formulation accounts for large increases in ultraviolet radiation associated with Antarctic ozone depletion. In *Ultraviolet Radiation and Biological Researach in Antarctica*, 39–42. Washington, D.C.

18. Madronich, S., McKenzie, R. L., Caldwell, M. M., & Björn, L. O. (1995). Changes in ultraviolet radiation reaching the Earth's surface. *Ambio, 24*(3), 143–152.

19. McKenzie, R. L., Aucamp, P. J., Bais, A. F., Bjoern, L. O., Ilyas, M., & Madronich, S. (2011). Ozone depletion and climate change: Impacts on UV radiation. *Photochemical & Photobiological Sciences, 10*(2), 182–198. https://doi.org/10.1039/c0pp90034f

20. Micheletti, M. I., & Piacentini, R. D. (2003). Sensitivity of biologically active UV radiation to stratospheric ozone changes: Effect of action spectrum shape and wavelength range. *Photochemistry and Photobiology, 78*(5), 456–461. https://doi.org/10.1562/0031-8655(2003)078%3c0456:sobaur%3e2.0.co;2

21. Seckmeyer, G., Bais, A., Bernhard, G., Blumthaler, M., Booth, C. R., Lantz, K., & McKenzie, R. L. (2008). *Instruments to measure solar ultraviolet irradiance. Part 2: Broadband instruments measuring erythemally weighted solar irradiance*. Vol. WMO TD No. 1289, WMO, Global Atmospheric Watch, Vol. 164. World Meteorological Organisation, Geneva.

22. McKenzie, R. L., Matthews, W. A., & Johnston, P. V. (1991). The relationship between erythemal UV and ozone derived from spectral irradiance measurements. *Geophysical Research Letters, 18*(12), 2269–2272. https://doi.org/10.1029/91GL02786

23. Bodhaine, B. A., Dutton, E. G., Hofmann, D. J., McKenzie, R. L., & Johnston, P. V. (1997). Spectral UV measurements at Mauna Loa: July 1995-July 1996. *Journal of Geophysical Research, 102*(D15), 19–273. https://doi.org/10.1029/97JD01391

24. Blumthaler, M., Salzgeber, M., & Ambach, W. (1995). Ozone and ultraviolet-B irradiances: Experimental determination of the radiation amplification factor. *Photochemistry and Photobiology, 61*(2), 159–162. https://doi.org/10.1111/j.1751-1097.1995.tb03954.x

25. Antón, M., Cazorla, A., Mateos, D., Costa, M. J., Olmo, F. J., & Alados-Arboledas, L. (2015). Sensitivity of UV erythemal radiation to total ozone changes under different sky conditions: Results for Granada, Spain. *Photochemistry and Photobiology, 91*, 215–219. https://doi.org/10.1111/php.12539 Epub 2015 Nov 4.

26. Hall, E. S. (2017). Comparison of five modeling approaches to quantify and estimate the effect of clouds on the radiation

amplification factor (RAF) for solar ultraviolet radiation. *Atmosphere*. https://doi.org/10.3390/atmos8080153

27. Molina, L. T., & Molina, M. J. (1986). Absolute absorption cross-sections of ozone in the 185 to 350 nm wavelength range. *Journal of Geophysical Research, 91*(D13), 14501–14508.

28. CIE (1998). *Erythema reference action spectrum and standard erythema dose*. CIE Standard, Vol. ISO 17166:1999(E), CIE DS 007.1/E-1998. Commission Internationale de l'Eclairage, Vienna, Austria.

29. Setlow, R. B., Grist, E., Thompson, K., & Weatherhead, A. (1993). Wavelengths effective in induction of malignant melanoma. *Proceedings of the National Academy of Sciences, USA, 90*, 6666–6670.

30. Bouillon, R., Eisman, J., Garabedian, M., Holick, M., Kleinschmidt, J., Suda, T., Terenetskaya, I., & Webb, A. (2006). *Action spectrum for the production of previtamin D3 in human skin, 2006*. UDC: 612.014.481–06 ed., Vol. 174:2006. CIE, Vienna.

31. McKenzie, R. L., Liley, J. B., & Björn, L. O. (2009). UV radiation: Balancing risks and benefits. *Photochemistry and Photobiology, 85*, 88–98. https://doi.org/10.1111/j.1751-1097.2008.00400.x

32. McKinlay, A. F., & Diffey, B. L. (1987). A reference action spectrum for ultra-violet induced erythema in human skin. In W. F. Passchier & B. F. M. Bosnajakovic (Eds.), *Human Exposure to Ultraviolet Radiation: Risks and Regulations* (pp. 83–87). Elsevier.

33. Webb, A. R., Slaper, H., Koepke, P., & Schmalwieser, A. W. (2011). Know your standard: Clarifying the cie erythema action spectrum. *Photochemistry and Photobiololgy*. https://doi.org/10.1111/j.1751-1097.2010.00871.x

34. Bais, A. F., McKenzie, R. L., Bernhard, G., Aucamp, P. J., Ilyas, M., Madronich, S., & Tourpali, K. (2015). Ozone depletion and climate change: Impacts on UV radiation. *Photochemical & Photobiological Sciences, 14*(1), 19–52. https://doi.org/10.1039/C4PP90032D

35. Bernhard, G., Mayer, B., Seckmeyer, G., & Moise, A. (1997). Measurements of spectral solar UV irradiance in tropical Australia. *Journal of Geophysical Research, 102*(D7), 8719–8730.

36. Norval, M., Björn, L. O., & de Gruijl, F. R. (2009). Is the action spectrum for UV-induced production of previtamin D3 in human skin correct? *Photochemical & Photobiological Sciences, 9*, 11–17. https://doi.org/10.1039/B9PP00012G

37. Holick, M. (1995). Environmental factors that influence the cutaneous production of vitamin D. *The American Journal of Clinical Nutrition, 61*, 638S-645S. https://doi.org/10.1093/ajcn/61.3.638S

38. Young, A. R., Morgan, K. A., Harrison, G. I., Lawrence, K. P., Petersen, B., Wulf, H. C., & Philipsen, P. A. (2021). A revised action spectrum for vitamin D synthesis by suberythemal UV radiation exposure in humans in vivo. *PNAS, Proceedings of the National Academy of Sciences, USA, 118*(40), e2015867118. https://doi.org/10.1073/pnas.2015867118

39. McKenzie, R. L., Johnston, P. V., & Seckmeyer, G. (1997). UV spectro-radiometry in the network for the detection of stratospheric change (NDSC). In C. S. Zerefos & A. F. Bais (Eds.), *Solar ultraviolet radiation modelling, measurements and effects* (pp. 279–287). Springer-Verlag.

40. McKenzie, R., Kotkamp, M., Liley, B., Disterhoft, P., & Bernhard, G. Long term variability and cloud effects in UV irradiances from NDACC spectrometers. In R. McKenzie (Ed.), *NIWA UV Workshop. UV Radiation: Effects on Human Health and the Environment, Wellington, New Zealand, 4–6 April 2018* https://www.niwa.co.nz/atmosphere/uv-ozone/uv-science-workshops/2018-uv-workshop

41. Stamnes, K., Slusser, J., & Bowen, M. (1991). Derivation of total ozone abundance and cloud effects from spectral irradiance measurements. *Applied Optics, 30*, 4418–4426.

42. Madronich, S., & Flocke, S. (1998). The role of solar radiation in atmospheric chemistry. In P. Boule (Ed.), *Handbook of Environmental Chemistry* (pp. 1–26). Springer-Verlag.

43. Bodeker, G. E., Tradowsky, J. S., Kremser, S., Schwertheim, A., & Lewis, J. (2021). A global total column ozone climate data record. *Earth System Science Data, 13*, 3885–3906. https://doi.org/10.5194/essd-13-3885-2021

44. McKenzie, R., Liley, B., & Disterhoft, P. Peak UV: Spectral contributions from cloud enhancements. In *International Radiation Symposium, Auckland, NZ, 20 April 2016* (Vol. 1810, AIP Conference Proceedings (2017)): AIP. https://doi.org/10.1063/1.4975570

45. Gröbner, J., Schill, H., Egli, L., & Stübi, R. (2021). Consistency of total column ozone measurements between the Brewer and Dobson spectroradiometers of the LKO Arosa and PMOD/WRC Davos. *Atmospheric Measurement Techniques, 14*, 3319–3331. https://doi.org/10.5194/amt-14-3319-2021

46. Morgenstern, O., Frith, S. M., Bodeker, G. E., Fioletov, V., & van der A, R. J. (2021). Reevaluation of total-column ozone trends and of the effective radiative forcing of ozone-depleting substances. *Geophysical Research Letters*. https://doi.org/10.1029/2021gl095376

47. Basher, R. E. (1982). *Review of the Dobson Spectrophotometer and its Accuracy. WMO Global Ozone Research and Monitoring Project*. WMO Report No. 13.

48. Vanicek, K. (2006). Differences between ground Dobson, Brewer and satellite TOMS-8, GOME-WFDOAS total ozone observations at Hradec Kralove, Czech. *Atmospheric Chemistry and Phyics, 6*, 5163–5171. https://doi.org/10.5194/acp-6-5163-2006

49. McKenzie, R., Bernhard, G., Liley, B., Disterhoft, P., Rhodes, S., Bais, A., Morgenstern, O., Newman, P., Oman, L., Brogniez, C., & Simic, S. (2019). Success of Montreal Protocol demonstrated by comparing high-quality UV measurements with "World Avoided" calculations from two chemistry-climate models. *Scientific Reports, 9*(1), 12332. https://doi.org/10.1038/s41598-019-48625-z

50. Zempila, M. M., van Geffen, J. H. G. M., Taylor, M., Fountoulakis, I., Koukouli, M. E., & van Weele, M. (2017). TEMIS UV product validation using NILU-UV ground-based measurements in Thessaloniki, Greece. *Atmospheric Chemistry and Physics, 17*, 7157–7174. https://doi.org/10.5194/acp-17-7157-2017

51. Fitzpatrick, T. B. (1988). The validity and practicality of Sun-reactive skin types I through VI. *Archives of Dermatology, 124*, 869–871.

52. McKenzie, R. L., Bodeker, G. E., Scott, G., & Slusser, J. (2006). Geographical differences in erythemally-weighted UV measured at mid-latitude USDA sites. *Photochemical & Photobiological Sciences, 5*(3), 343–352. https://doi.org/10.1039/b510943d